



Analyses and design of steep slope with GeoBarrier system (GBS) under heavy rainfall

Hariato Rahardjo^{a,*}, Yongmin Kim^a, Nurly Gofar^{a,b}, Alfredo Satyanaga^a

^a School of Civil and Environmental Engineering, Nanyang Technological University, Block N1, #19-26, 50 Nanyang Avenue, Singapore, 639798

^b Postgraduate Program Universitas Bina Darma, Jl. Jendral Ahmad Yani, Palembang, Indonesia

ARTICLE INFO

Keywords

GeoBarrier system (GBS)
Reinforced soil wall
Capillary barrier
Suction contribution

ABSTRACT

A GeoBarrier system (GBS) is a combination system of reinforced soil walls to stabilize near-vertical cut slopes and capillary barrier principles to protect the wall from the effect of rainfall infiltration. Singapore requires construction materials that are cost-effective to support sustainable urban development. Therefore, recycled materials are utilized as GBS materials to avoid the use of high-cost materials, such as steel or concrete. GBS consists of planting geobags with unique geosynthetic pockets for sustainable plant species as a facing layer of GBS. The negative pore-water pressure (suction) within the reinforced soil behind GBS was assured to be constant during rainfall since GBS is designed specially to minimize the rainfall infiltration into the reinforced soil. This paper presents the practical design and stability analysis of the GBS, considering the presence of suction within the reinforced soil body. The monitoring of GBS performance in the field was carried out via field instrumentation. Finite element analyses of the GBS under extreme rainfalls were also performed for evaluation of the GBS performance. The field instrumentations and numerical analysis results showed that GBS was able to protect the slope from rainfall infiltration; therefore, the stability of the slope retained by GBS was not affected by the rainfall. Results from the analytical calculation showed that the most critical mode of failure is sliding along the base, followed by the global and local slope stability. The GBS is not susceptible to local instability.

1. Introduction

Singapore is considered densely populated, with 5.5 million people living within 720 km² area (Singapore Dept of Statistic, 2015). One solution to this issue is to construct building underground for creating a new space. Concrete retaining structures are commonly used for underground constructions. As a result, the total cost of construction will be high and concrete walls can be aesthetically poor without possibility of growing vegetation. Rahardjo et al. (2018) introduced an innovative retaining structure, GeoBarrier system (GBS), for a replacement of concrete retaining walls. This new system combines capillary barrier system (CBS) with geobags which are fabricated from geosynthetics. The bags encapsulate the materials of GBS to avoid sliding issues. The study by Matsuoka et al. (2001) indicated that the soils contained insides geosynthetic bag can increase strength of the reinforced soil wall. The use of geobags also provides an environmentally friendly retaining wall, which is an alternative to reinforced soil wall with low cost (Ansari et al., 2011).

Matsuoka and Liu (2006) showed that geobags could be used as a retaining wall in different locations in Japan. However, the use of reinforced soil wall including geobag retaining wall is not widely accepted by many engineers in the world (Lee et al., 2010; Ren et al., 2018

). This is partly attributed to the occurrence of failures of this system in several areas in the world (Yoo, 2011; Yoo and Jung, 2006), which are mainly caused by the limitation of the drainage system and the use of improper fine-grained soil (Koerner and Soong, 2011). Therefore, it is necessary to develop a new geobag retaining structure with an effective drainage system utilizing non-cohesive materials.

The principles of GBS are the same as CBS, with additional geobag and reinforcement to retain the steep slope behind it. The CBS is commonly used as cover system to stabilize the slope (Rahardjo et al., 2012, 2013a,b) and to protect the landfill (Nicholson et al., 1989; Ross, 1990) where the permeability of coarse-grained material is much lower than the permeability of fine-grained material in unsaturated conditions (Stormont and Anderson, 1999; Khire et al., 2000). These contract characteristics in hydraulic properties are required to minimize water infiltration into the soil beneath CBS (Tami et al., 2004). The schematic diagram of the GBS is presented in Fig. 1. GBS incorporates recycled materials within the fine- and coarse-grained layers to achieve environmental sustainability. Combinations of fine and coarse recycled materials with recycled concrete aggregates (RCA) and reclaimed asphalt pavement (RAP) were used in the study. The geobag containing fine RCA or fine RAP is placed on top of each other to form the GBS retaining wall. The coarse RCA or coarse RAP is laid between reinforced soil and fine RCA or fine RAP geobag to pro-

* Corresponding author.

E-mail addresses: chrahardjo@ntu.edu.sg (H. Rahardjo); kimkimym@ntu.edu.sg (Y. Kim); nurly_gofar@binadarma.ac.id (N. Gofar); Alfredo@ntu.edu.sg (A. Satyanaga)

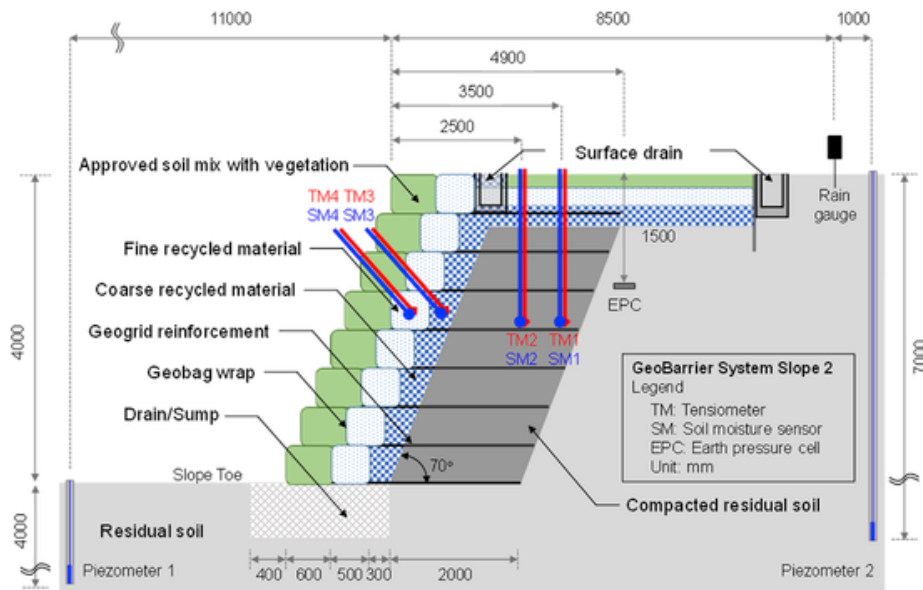


Fig. 1. Schematic diagram of GeoBarrier System (GBS) slope 2 as with instrumentations.

vide the barrier system for minimizing water infiltration into the compacted residual soil. Approved soil mix (ASM) was encapsulated inside geobag and placed in front of the RCA or RAP layer.

This paper focuses on the design calculation, and the stability analyses of the GBS constructed within a residual soil in Singapore. Unsaturated soil mechanics principles were considered by incorporating suction in the GBS design and stability analysis. Appropriate unsaturated soil properties and relevant formulas presented in Fredlund and Rahardjo (1993) were used in this study. The lateral earth pressure formula for analyses of cohesive soil (AASHTO, 2009; Berg et al., 2009) was integrated in the analyses to incorporate the transfer of stress into the reinforcing member.

2. Construction and performance of GeoBarrier system (GBS)

2.1. GBS components

Three slopes retained by GBS were constructed within the residual soil from Bukit Timah Granite in Singapore with the incorporation of fine RCA overlying coarse RCA in GBS slope 1, fine RAP overlying coarse RAP in GBS slope 2 and fine RCA overlying coarse RAP in GBS slope 3 (Figs. 1 and 2). The construction of slopes retained by GBS was carried out with a height of 4 m and a slope angle of 70°. The GBS consisted of 8 layers of geobags stacked on top of each other and supported with 2.8 m long of geogrid within each layer of geobag.

Geogrid was used as reinforcements that were securely connected to the bags of ASM and fine RCA/fine RAP. The initial characteristic strength at 5% strain of the geogrid was 34.4 kN/m, and the unit weight was 0.25 kg/m². The geogrid has a 60 kN/m characteristic strength (σ_{ult}) and 4 mm thickness (t). A 0.3-m thick of coarse material (coarse RCA/coarse RAP) was compacted on top of the compacted residual soil as the reinforced soil fill to achieve the required density of 1.7 Mg/m³. The wall face was made of geobags (0.5 m × 0.5 m) filled with fine RCA and geobags of ASM of 0.6 m × 0.5 m size. The ASM bags are used on the wall face for growing plants. The combination of geobags of ASM and fine RCA forms a gabion type of facing of 1.1 m thick. During the filling process, the geobag was placed within a wooden box with a similar size as the designed geobags for fine RAP and coarse RAP to ensure the integrity of the geobag prior to lifting and placement of geobags in the GBS location.

2.2. Material properties

Fine RAP and coarse RAP were utilized as GBS materials in this study. The residual soil retained by the GBS was classified as a highly plastic clay (CH) following the Unified Soil Classification System (USCS) (ASTM D2487). The summary of index properties of the GBS materials and residual soil investigated in this study is given in



Fig. 2. Pilot study of GeoBarrier System (GBS) with three different material combinations.

Table 1. The fine RAP and the coarse RAP are classified as Poorly graded sand (GP) and Poorly graded gravel (SP), respectively. Fig. 3 presents the grain-size distributions of fine RAP, coarse RAP, ASM, and residual soil.

The measurements of soil-water characteristic curve (SWCC) of GBS materials and residual soil were carried out following the relevant ASTM standards (ASTM D6838). The permeability functions were derived from SWCCs. The SWCCs and permeability functions of the GBS materials and the residual soil are presented in Fig. 4. Note that air-entry values were inferred from Zhai and Rahardjo (2012) equations. Fine RAP and coarse RAP have a water-entry value, Ψ_w of 50 kPa and 0.8 kPa, respectively. The ratio of water-entry value between fine and coarse RAP was 62.5, which was much higher than 10 (one of the criteria for satisfactory capillary barrier performance based on the study from Rahardjo et al., 2013a,b). The saturated coefficients of permeability, k_s , for fine RAP and coarse RAP are 1.2×10^{-6} m/s and 4.0×10^{-3} m/s, respectively. The k_s of coarse RAP was in accordance with the requirement proposed by Rahardjo et al. (2013a,b), which was equal to or higher than 1.0×10^{-5} m/s to ensure the effectively continuous flow of water within the GBS materials. The hydraulic and shear strength properties of the GBS materials and the residual soil are presented in Table 2.

Table 1
Index properties of materials used in seepage analyses.

Properties	Residual Soil	Fine RAP	Coarse RAP
USCS classification	CH ¹⁾	SP ²⁾	GP ³⁾
Specific gravity, G_s	2.61	2.57	2.66
Porosity, n	0.440	0.390	0.437
Unit weight, γ_t (kN/m ³)	20.3	19.0	20.0
Natural water content, w (%)	38	6.70	6.56
Optimum water content, w_{opt} (%)	11	NA	NA

1) Highly plastic clay.
2) Poorly graded gravel.
3) Poorly graded sand.

2.3. Field instruments and monitoring

The rainfall and groundwater table variations within the GBS slope area in this study were monitored using a rain-gauge and two Casagrande-type piezometers, respectively. The changes in negative pore-water pressure (PWP) was monitored using four pairs of the tensiometer, while the fluctuations in volumetric water content (VWC) was monitored using four pairs of soil moisture sensor. The tensiometers and soil moisture sensors were installed at 2 m depth from the ground surface in the crest of the slope. Each of the instruments was installed within the different GBS materials (reinforced soil, coarse material, and fine material) in order to monitor the responses of PWP and VWCs within the different GBS layers and the compacted residual soil during rainfalls. Hence, the breakthrough of rainwater into the coarse-grained layer or the compacted residual soil behind GBS can be monitored. In other words, the performance of GBS to minimize rainwater infiltration can be monitored in real-time.

This paper presents the response of the middle slope (GBS slope 2) because earth pressure cells were also installed in GBS slope 2 to monitor transient vertical and lateral stresses against the rainwater infiltration. The earth pressure cells were located at 1.5 m depth from the ground surface on the crest of the slope. Data acquisition system (DAS) with an internet connection was connected to all instruments for on-line and real-time monitoring. The schematic diagram of GBS slopes with the locations of the instruments is indicated in Fig. 1.

The monitoring period was one year from 1st July 2016 to 30th June 2017. Special attention was given to the rainfall record for January 2017 (Fig. 5) where one week of rainfall was observed after the occurrence of a long dry period. The total rainfall amount from 18th January 2017 until 23rd January 2017 was 204 mm, where the highest amount of rainfall intensity was 103.8 mm/day and 38.7 mm/h (at 10:00 a.m.) on 23rd January 2017.

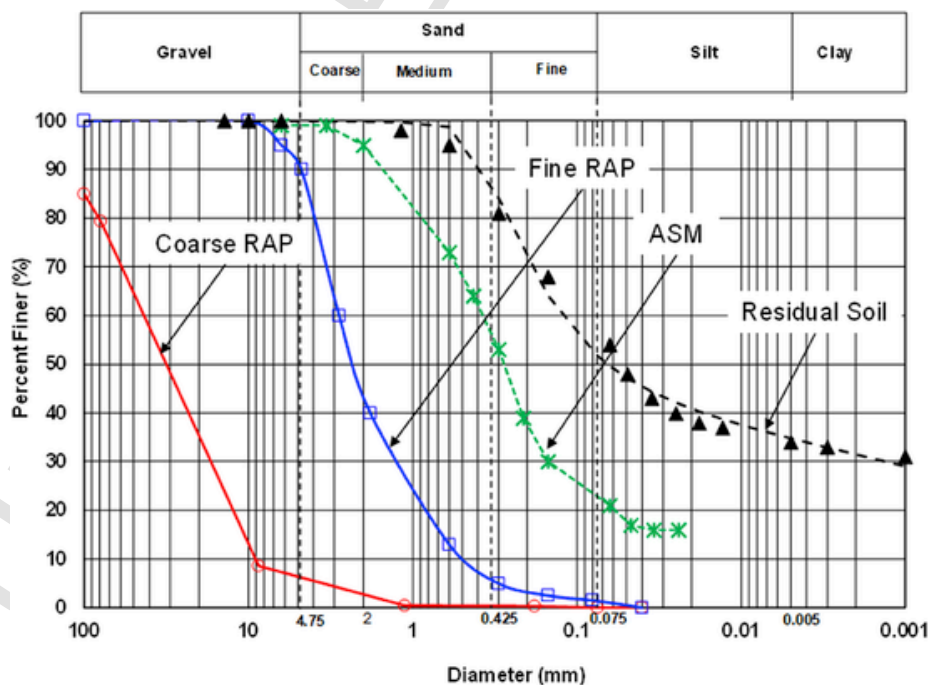
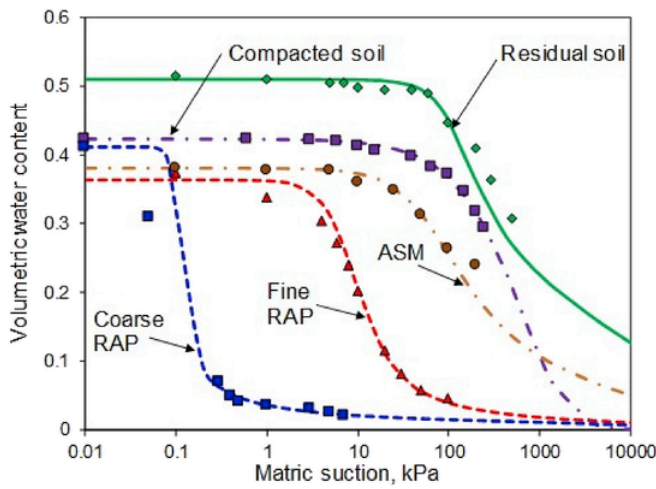
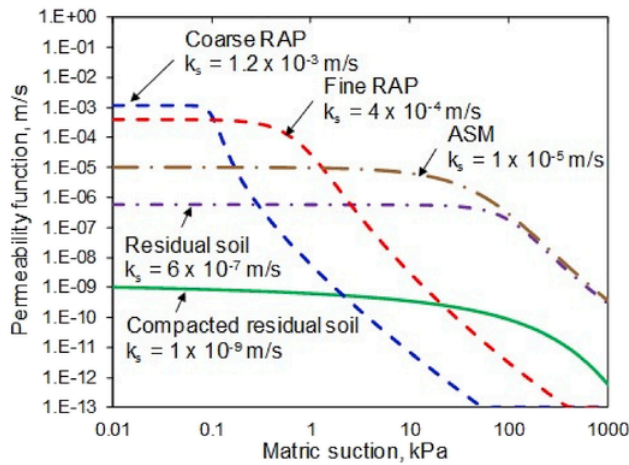


Fig. 3. Grain-size distribution of RAPs, ASM, and residual soil for GBS slopes.



(a) SWCCs



(b) Permeability functions

Fig. 4. Unsaturated properties of materials used for GBS slopes.

2.4. Field monitoring results and GBS performance

The changes in PWP within GBS layers and the compacted residual soil are presented in Fig. 6. It was observed that the PWP within the compacted residual soil was almost constant, between -18 and -22 kPa, suggesting very minimum rainwater percolated down into the compacted residual soil during rainfall. Similarly, no changes in

PWPs were observed within the coarse-grained layer (-4.5 kPa). The slight fluctuations in PWP were also monitored within the fine-grained layer (between -14.5 and -16.5 kPa). Pore water pressure responses showed that no breakthrough occurred during heavy rainfalls between January 18th and 23rd, 2017. Field instrumentation data also indicated a constant vertical and horizontal pressures in GBS slope 2 during rainy periods (Fig. 7). It indicated that there was no influence of water infiltration on the compacted residual soil behind the GBS during rainfall. In other words, the GBS was able to protect the slope from rainfall infiltration. Hence, the stability of the slope could be maintained during heavy rainfalls.

3. Analytical calculation of GeoBarrier system (GBS)

3.1. External stability

In general, the external stability of a retaining wall was evaluated against bearing capacity issue, overturning, sliding, and overall stability of a slope. Koerner (2005) studied that overturning is not a problem in reinforced walls since the bending moment cannot be mobilized due to the inherent flexibility. In addition, a reinforced soil wall is a light structure as compared to a gravity wall or even a concrete cantilever wall. Thus the shear failure of the foundation soil, as well as excessive settlements, are not of concern. Hence, the overall stability of the GBS is usually governed by sliding along the base and slope instability.

The evaluation of GBS stability against sliding requires the estimation of lateral earth pressure in active condition. The coefficient of active lateral earth pressure based on the unsaturated soil formulation (Fredlund et al., 2012) is as follows:

$$K_{as} = \frac{1}{N_\phi} - \frac{2c'_s}{\sigma_v} \frac{1}{\sqrt{N_\phi}} - 2 \frac{\psi}{\sigma_v} \tan \phi^b \frac{1}{\sqrt{N_\phi}} \tag{1}$$

where $N_\phi = \tan^2 (45 + \phi'/2)$ is the coefficient of passive earth pressure, c'_s and ϕ'_s are effective shear strength properties of the foundation soil, $\psi = (u_a - u_w)$ is matric suction, $\sigma'_v = (\sigma_v - u_a)$ is net normal stress, ϕ^b is the internal friction angle with respect to matric suction u_w and u_a are pore water and pore air pressure in the soil.

Wright and Duncan (1991) proposed to use Bishop's simplified method in analyzing the stability of steep reinforced slopes. Formulations for stability analysis based on moment and force equilibriums of unsaturated soil slope where the pore-air pressure is atmospheric are as follows (Fredlund et al., 2012):

$$F_{mf} = \frac{\sum [c'b + (N - u_w b) \tan \phi'] R}{A_L \alpha_L + \sum Wx} \tag{2}$$

$$F_{ff} = \frac{\sum [c'b \cos \alpha + (N - u_w b \frac{\tan \phi^b}{\tan \phi'}) \tan \phi' \cos \alpha]}{A_L + \sum N \sin \alpha} \tag{3}$$

Table 2

Hydraulic and shear strength properties of materials used in this study.

Description	ASM	Residual soil	Fine RAP	Coarse RAP	Gravel	Compacted residual soil
Effective cohesion, c' (kPa)	2	5	0	0	0	5
Effective friction angle, ϕ' (°)	30	28	34	35	35	38
Air-entry value, ψ_a (kPa)	26	64	0.40	0.09	0.07	112.5
ϕ^b (°) for $0 < \psi \leq \psi_a$	30	28	34	35	35	38
ϕ^b (°) for $\psi > \psi_a$	15	14	17	17	17	14
Total unit weight, γ (kN/m ³)	16.5	18.0	20.0	21.0	21.0	20.0
Saturated volumetric water content, θ_s	0.381	0.51	0.364	0.412	0.39	0.423
Saturated permeability, k_s (m/s)	1×10^{-5}	1×10^{-7}	4×10^{-4}	1.2×10^{-3}	5×10^{-1}	1×10^{-9}

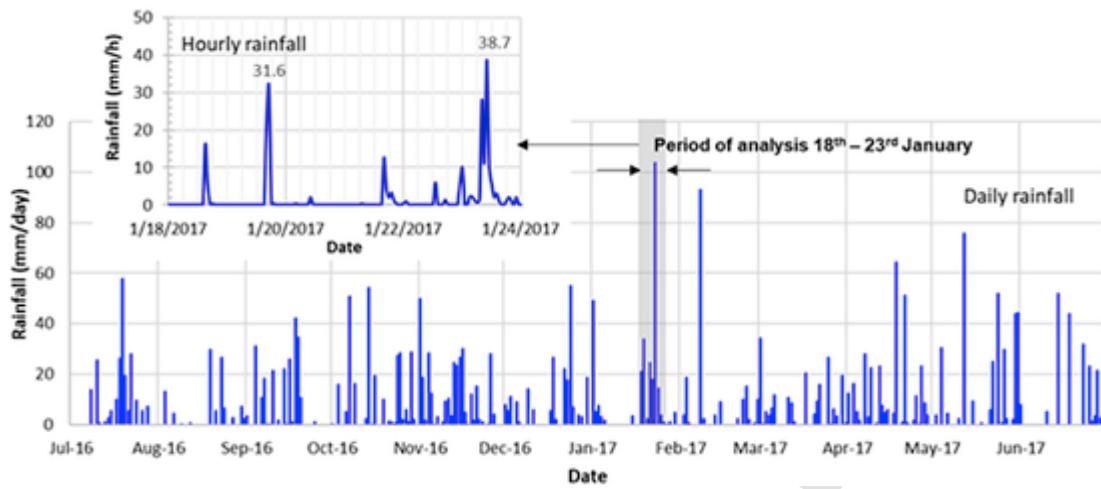


Fig. 5. Rainfall records from a year monitoring period (1st July 2016–30th June 2017) and the rainfall condition analyzed in this study (18th January to 23rd January 2017).

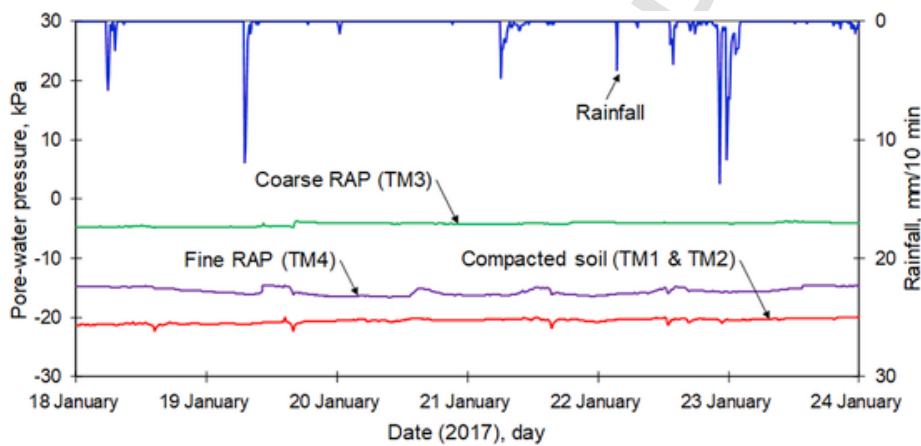


Fig. 6. PWP variations from field instrumentations in GBS slope 2 between 18th January and 23rd January 2017.

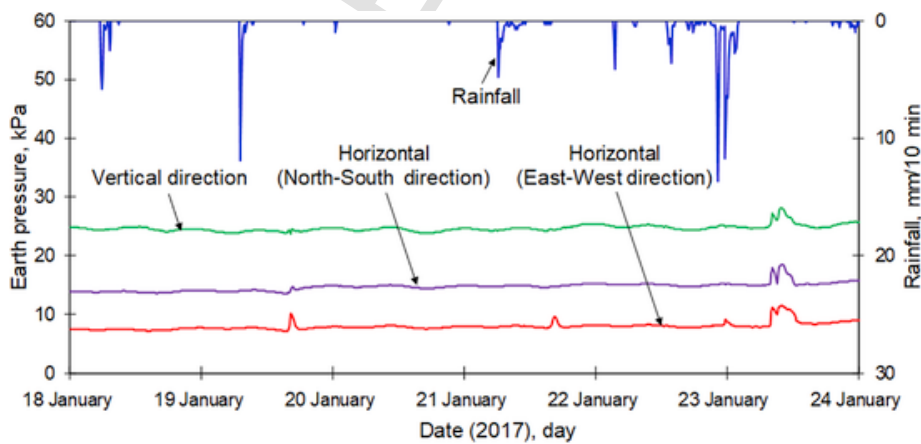


Fig. 7. Effect of rainwater infiltration on vertical and horizontal pressures in GBS slope 2 between 18th January and 23rd January 2017.

where F_{mf} and F_{ff} are the factors of safety with respect to moment and force equilibrium, b is the width of the slice, N is the normal force, α is the angle between the tangent to the center of the base of each slice and the horizontal, A_L is the resultant of external water force, while other parameters are as defined previously. For reinforced slope, each layer of reinforcement can be represented by a concentrated force applied along slip surface as shown in Fig. 8 and can be computed

based on the analytical procedure given in Koerner (2005) or using slope stability program such as SLOPE/W (GEO-SLOPE, 2012).

3.2. Internal stability

The analyses of the internal stability of GBS wall were carried out by comparing the reinforcement load with the tensile strength of the reinforcement (geogrid) as well as the friction that occurred be-

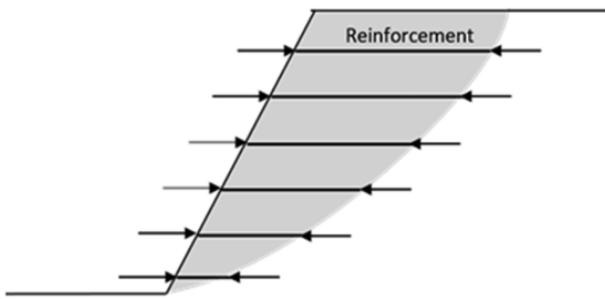


Fig. 8. Reinforcement force used in the internal stability analysis of reinforced soil slope (Wright and Duncan, 1991).

tween the geogrid and the compacted residual soil. The available factor of safety ($FoS_{tensile}$), the ratio between the reinforcement (T_{max}) and the ultimate strength of the reinforcement (T_u), should be higher than the material reduction factors (functions of the reinforcement installation damage (FC), the effects of creep (FD), and the effects of environment (FS)) (Koerner, 2005; Berg et al., 2009).

$$FoS_{tensile} = (T_u/T_{max}) \geq (FC \times FD \times FS) \quad (4)$$

Berg et al. (2009) observed that the reinforcement type influences the mechanism of stress transfer between the reinforcement and the soil. For a geogrid reinforcement with opening $>d_{50}$ of the reinforced soil, the stress transfer could be estimated as $P_r = 2F^* \delta \sigma'_v L_e$ for which $\delta = 0.8$ while F^* represents the stress transfer mechanism between the reinforced soil and geosynthetics. For geogrids with opening $>d_{50}$ of the reinforced soil $F^* = \tan \varphi_{sg} = \frac{2}{3} \tan \varphi_s$ for which φ_s is the angle of internal friction of the reinforced soil. The required anchorage length of geosynthetics reinforcement (L_e) is as follows:

$$L_e = (\sigma'_v \times 2/3 \tan \varphi_r \times \alpha \times A) / \tau_{max} \quad (5)$$

where A is the area retained by geogrids, τ_{max} is the maximum pullout capacity of geogrids, σ'_v is overburden pressure (σ'_v).

Thus, the factor of safety with respect to pull-out is:

$$FoS_{tensile} = (L_a/L_e) \quad (6)$$

where L_a is the pull-out capacity.

3.3. Stress transferred to reinforcing element

The maximum tensile stress in reinforcing elements can be estimated using three different methods, i.e. based on slope stability analysis (Wright and Duncan, 1991), as given in Fig. 9; the existing design guidelines or simplified method (AASHTO, 2009; Berg et

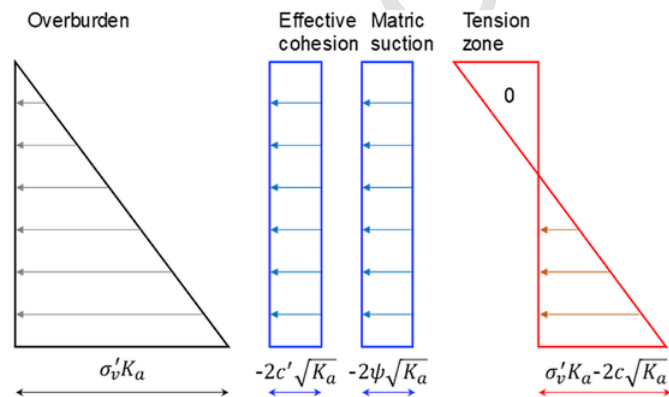


Fig. 9. Active earth pressure distribution in unsaturated soil if suction is constant with depth (Fredlund et al., 2012).

al., 2009) and the simplified stiffness method (Allen and Bathurst, 2015). As shown by Gofar and Hanafiah (2018), the methods gave comparable results in terms of stress transferred to the reinforcing element.

In the simplified methods (AASHTO, 2009; Berg et al., 2009), the maximum tensile or pull-out force (T_{max}) resisted by a reinforcing element is the integration of horizontal stress within the contributory area of the reinforcement layer. For a geosynthetic reinforcement, the tributary area is equal to the vertical spacing between two reinforcing layers (S_v):

$$T_{max} = \sigma'_h \times S_v \quad (7)$$

The effective horizontal earth pressure against the wall (σ'_h) with cohesive backfill is as follows:

$$\sigma'_h = \sigma'_v K_a - (2c \sqrt{K_a}) \quad (8)$$

For an unsaturated soil, the total cohesion of soil is derived from soil's mineralogy, the effective cohesion (c') and the matric suction (ψ) as defined as follows (Fredlund et al., 2012):

$$c = c' + \psi \tan \varphi^b \quad (9)$$

where φ^b is an angle indicating the rate of increase in shear strength with respect to a change in matric suction. The distribution of the active pressure in unsaturated soil is presented in Fig. 9. Only positive pressure was considered in the analysis adopted in this study.

In this study, the effect of cohesion in the simplified method (Allen and Bathurst, 2015) was included with the incorporation of the cohesion in the horizontal stress calculation Equation (7). The most important factor evaluated in this study is the cohesion factor Φ_c . The effect of cohesion was first developed by Miyata and Bathurst (2007) and Bathurst et al. (2008) and then modified by Allen and Bathurst (2015) to the following form:

$$\Phi_c = e^{\lambda c / \gamma H} : 0 \geq \Phi_c \geq 1 \quad (10)$$

where λ is the cohesion coefficient ($= -16$), c is the total cohesion of the reinforced soil, including the effect of suction. The effective cohesion and the cohesion component resulting from matric suction or negative pore-water pressure can be measured for a particular soil. In this method, the cohesion factor is only applicable for soils with plasticity index (PI) > 6 .

The analytical calculation was carried out based on the geometry and the materials used in this study as well as the soil properties of GBS constructed in the residual soil of Singapore, as presented in Section 2. The modulus of wall facing was derived from the combined modulus of fine RAP and ASM in proportion to their thicknesses, which are 0.5 m and 0.6 m respectively. The combined elastic modulus of the wall facing (57000 kPa) was determined from the slope of the stress-strain curve of the GBS materials. The shear strength parameters of the reinforced soil used in the analysis are $c' = 5$ kPa and $\varphi' = 38^\circ$ while the unit weight is 20 kN/m³. The φ^b angle was 14° . The wall was reinforced with geogrids with a vertical spacing of 0.5 m and a reinforcement length of 2.8 m or 0.7 times of the wall height. The geogrids were securely connected to the bags of ASM and fine RAP. The initial characteristic strength of the geogrids, defined as the load resistance at 5% strain, was 34.4 kN/m, while the modulus of the geogrids (J) was 600 kN/m. Since the geogrids were to be in contact with the coarse-grained material near the wall face (Fig. 1), the characteristic strength should be reduced to a factor related to the installation damage $FC = 1.10$. The required service life considered in this study is 60 years, thus material reduction factors related to creep effects FD and the environmental effects FS were 1.41 and 1.03, respectively. The effective friction surface between the geogrids and the reinforced soil (α) is

0.4. The analysis was performed for a surcharge weight of 10 kPa on the crest to simulate a nominal surcharge load that may occur during the service life of the wall (Berg et al., 2009). Suction variation from 0 to 50 kPa in both the foundation and reinforced soil was considered at increments of 10 kPa. All analyses were performed using a spreadsheet program in Microsoft Excel environment.

The force in the geogrids layer varies from close to zero at the crest to a maximum value at a depth of 1.5 m. The force is constant from depth of 1.5 m to maximum depth of 4 m. The variation of maximum force with matric suction, shown in Fig. 10 indicated that the force decreases with increasing apparent cohesion derived from suction, which is in agreement with Allen and Bathurst's (2015) statement that the tensile force in reinforcement decreases due to suction. External stability analyses showed that sliding along the base was the most critical mode of external failure with factor of safety (FoS) against sliding increasing from 1.36 for $\psi = 0$ to 1.59 for $\psi = 50$ kPa. The FoS for global slope stability increases from 1.75 to 2.63 as suction increases from 0 to 50 kPa, while the FoS for local slope stability is slightly higher in a saturated condition ($\psi = 0$ kPa), i.e., 1.89 and it increases to 2.25 when suction increases to 50 kPa. The variations of FoS for sliding along the base as well as local and global slope stability with suction are shown in Fig. 11. For internal stability analysis, the allowable tensile resistance (T_{all}) was 18.8 kN while the pull-out resistance is a function of overburden pressure at the level of the geogrid reinforcement and thus varies with depth. The variations of the minimum FoS against tensile and pull-out failure are also shown in Fig. 11.

4. Numerical analyses

4.1. Coupled deformation-seepage model

A two-dimensional (2D) coupled deformation-seepage numerical model was developed using SIGMA/W (GEO-SLOPE, 2012) to examine the response of a GeoBarrier System (GBS) under severe rainfall conditions in Singapore. The finite element mesh and boundary conditions of two (2) cases are illustrated in Fig. 12. In the first case, a typically steep slope of a 4 m high with an inclination angle of 70° was covered with geobags that are filled with the residual soil and reinforced with geogrids used in this study as shown in Fig. 12 (a). The simulated steep slope consists of the residual soil from the Jurong Formation in Singapore. In the second case shown in Fig. 12 (b), the slope is reinforced with the GBS and the geogrids that are strongly attached to the geobags and extended to 2.8 m (70% of slope height) from

the GBS facing or 1.4 m behind the coarse reclaimed asphalt pavements (coarse RAP) layer. The GBS is comprised of the compacted residual soil (reinforced zone), geogrids, fine reclaimed asphalt pavements (fine RAP), and coarse RAP for the capillary barrier cover, and ASM for the sustainable green cover.

The boundaries between the GBS and the slope in the lateral direction were set to three times the slope height to avoid the influence of the lateral boundary conditions. The lateral boundaries of the slope are fixed against horizontal displacement, and the bottom boundary of the slope is fixed against both horizontal and vertical displacements. The construction sequence that started with a field geostatic condition and placement of geobags and reinforced soil was considered in the analysis to generate the proper stress condition of the slope prior to a rainfall event.

Groundwater table position was obtained from the piezometer reading (1.5 m below the ground surface at the toe of the slope) at the location. The initial hydraulic condition of the slope was taken based on the position of the groundwater table as a hydrostatic pore-water pressure condition. The maximum matric suction in the slope was set to 35 kPa to simulate the in-situ condition. The flux boundary (q) equal to a rainfall intensity of 4.09×10^{-6} m/s (14.7 mm/h) for 24 h was applied to the surface of the slope. This flux boundary was approximately around the maximum recorded daily rainfall in Singapore of 353.6 mm/day (Meteorological Service Singapore, 2015). In order to evaluate the effect of rainfall infiltration on the deformation of the GBS, the analyses were carried out during the periods with and without rainfall. First, a rainfall intensity of 4.09×10^{-6} m/s was applied on the surface of the slope for 24 h. Then no rainfall was used in the analyses for 72 h to allow the groundwater table recovery for subsequent analyses as shown in Fig. 13. The non-ponding condition was applied on the slope surface to avoid the generation of positive pore-water pressure at the ground surface. The total head (h_w) was applied to the lateral boundaries of the slope below the groundwater table. No flow boundaries were applied at the bottom and along the lateral side of the slope by assigning a nodal flux (Q) equal to zero. The nodal flux (Q) was taken to be zero with review at the outer boundaries of the surface drain to drain out the collected rainwater.

4.2. Slope stability analyses

Slope stability analyses were also performed using SLOPE/W (GEO-SLOPE, 2012). The pore-water pressure distributions of the slope

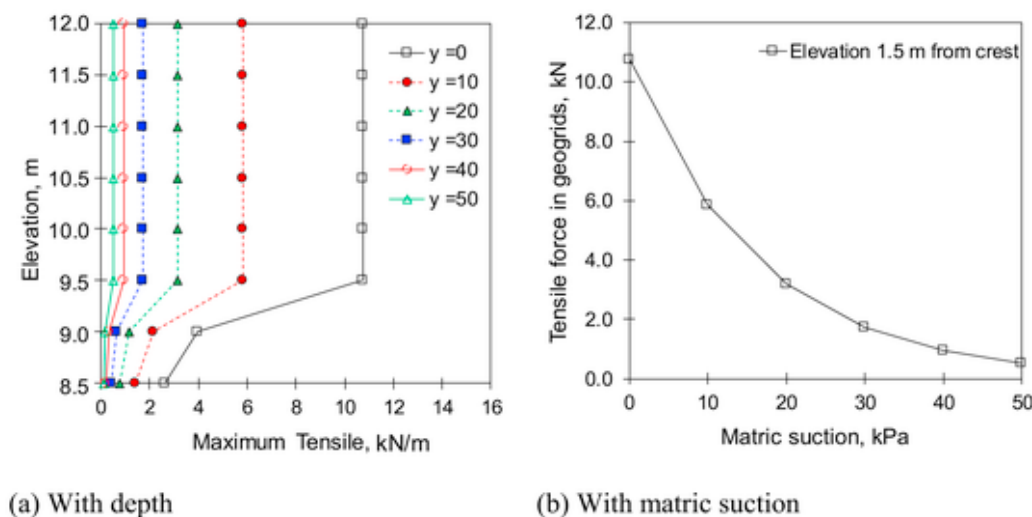


Fig. 10. Variation of maximum stress in geogrids.

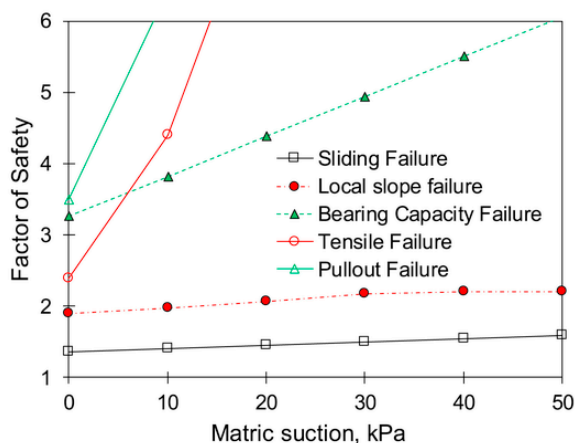


Fig. 11. Factor of safety variations for external and internal stability of GBS with matric suction.

culated from the coupled deformation-seepage analyses were imported to SLOPE/W. The shear strengths of both the saturated and unsaturated residual soils obtained from laboratory tests were used in the slope stability analyses based on Morgenstern-Price method (1965). The distributions of matric suction were selected and the factor of safety was calculated for every time increment.

In addition to the stability analysis of a slope, the deformation of the slope was incorporated in the slope stability analysis. First, the developed horizontal displacements were investigated at the three different locations (e.g., slope crest, slope midpoint, and slope toe). These locations corresponded to the locations of a critical slip surface obtained from the slope stability analyses. Second, dimensionless displacements ($E_s \delta_{max} / \gamma_t H^2$) were calculated to search for an inflection point, where E_s is Young's modulus of the soil, δ_{max} is the maximum displacement of the slope along the critical slip surface, γ_t is the unit weight, and H is the slope height (Kim et al., 2013). Two tangent lines were drawn on the relationship between the dimensionless displacement and the elapsed time to evaluate the slope instability. The intersection points of the two tangent lines represent the instability condition of the slope. Third, the maximum horizontal displacements along the critical slip surface with respect to the fluctuated rainfall were also investigated to study the effect of rainfall infiltration and to confirm the deformation characteristics of the slope due to rainfall infiltration. Fig. 14 illustrates the procedure of numerical analyses for evaluating the slope instability based on soil deformation characteristics and limit equilibrium criteria.

4.3. Results of numerical analyses

Variations in the factor of safety (FoS) calculated from the limit equilibrium analyses of the slope covered with geobags and GBS are shown in Fig. 15. The slightly higher initial FoS was observed in the slope with GBS (2.16) compared with the slope with geobags (2.05) due to the capillary barrier effects. However, the rate of decrease in FoS for the slope with geobags was faster than the slope with GBS. The FoS for the slope with geobags reached 1.49 at the end of the rainfall event while the FoS for the slope with GBS remained constant dur-

ing rainfall. As expected, the GBS has a significant effect on the slope stability under heavy rainfall events.

Fig. 16 shows the horizontal deformations at the three locations along the critical slip surfaces that were evaluated from SLOPE/W analyses (Fig. 17). The two simulated slopes exhibited higher horizontal displacements than vertical displacements. The deformation of the slope with geobags was higher than that of the slope with GBS. It is also shown that the slope with geobags exhibited typical deformed behavior of soil slopes while the slope with GBS represented the rigid behavior of retaining walls.

In order for the dimensionless displacement to define slope instability, horizontal displacements at the three locations, as mentioned earlier, were used in this study. The deformation characteristics represented by the relationship between the dimensionless displacement and elapsed time during the rainfall is shown in Fig. 18. Fig. 18 (a) shows that the dimensionless displacement of the slope with geobags increased during rainfall, especially rapid increase in the deformation was observed after 4 h. It can be said that the slope tended to be vulnerable right after the rainfall event. On the other hand, Fig. 18 (b) shows that the slope with GBS deformed relatively less than the slope with geobags. In addition, the deformation increments the GBS slope was not significant. Consequently, no evidence of the instability of the GBS slope was found in the relationship between the dimensionless displacement and time.

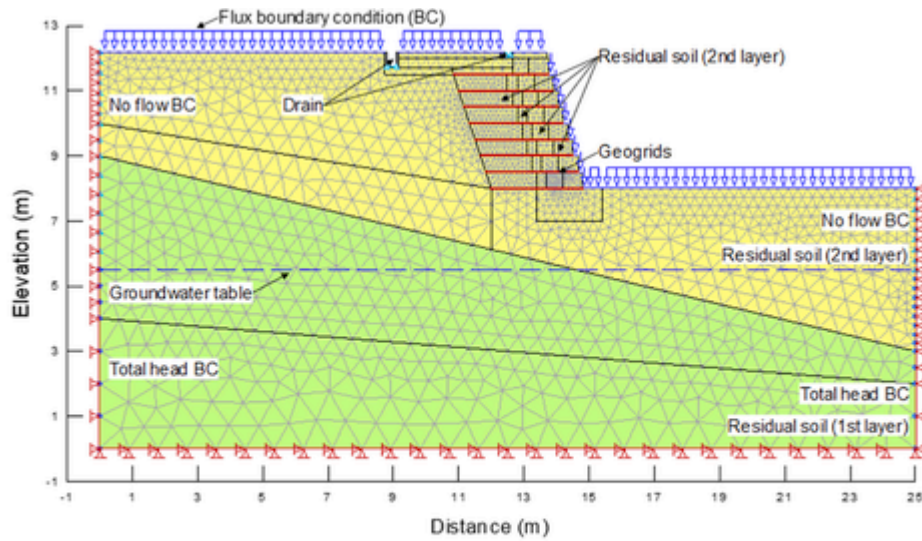
Fig. 19 shows the variations of horizontal deformation from the numerical analyses with the incorporation of a fluctuated rainfall event as depicted in Fig. 13. The figure shows that the increases in the lateral deformations were induced by rainfall for 24 h, and the deformations decreased gradually to the initial values during no rainfall conditions of 72 h when the groundwater table returned to the initial position. By repeating the rainfall event, the maximum lateral deformation developed at the three different locations increased slightly. However, the slope with GBS had smaller deformations compared with the slope with geobags, confirming the superiority of GBS with the effects of capillary barrier on the overall stability of the slope.

5. Conclusions

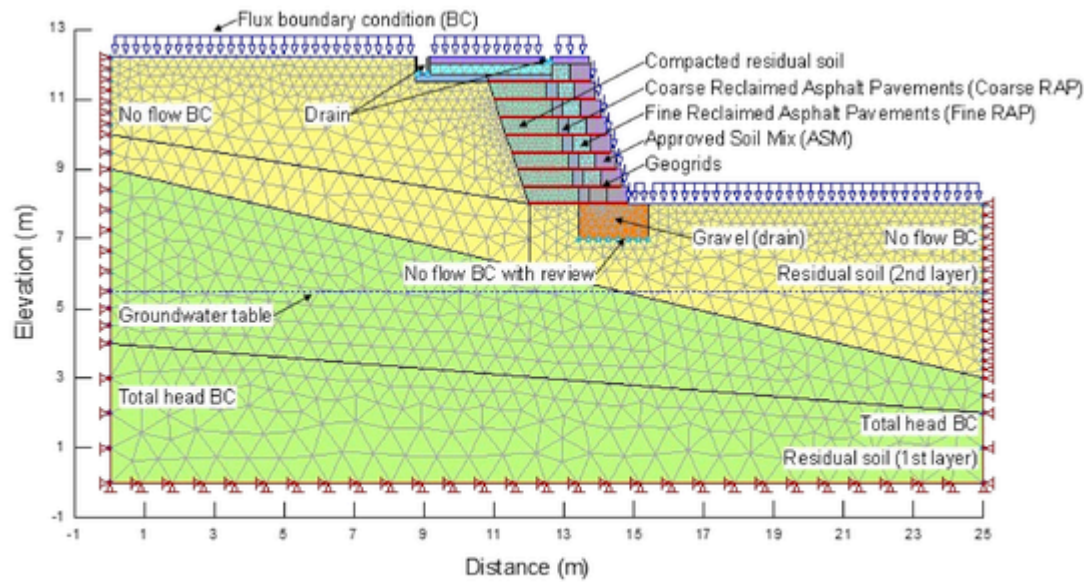
Available design and stability analysis methods of the reinforced retaining wall could be used for the newly developed GeoBarrier system (GBS) by incorporating unsaturated soil formulations in the methods. Stability analysis of GBS constructed in Singapore shows that the stability of the wall increases with suction. The most critical mode of the external failure is sliding along the base, followed by the global and local slope stability. Due to its flexibility, the GBS is not susceptible to overturning as well as the shear failure of foundation soil and excessive settlement. The fact that the maximum tensile stress in the reinforcement decreases with matric suction implies that the geogrid reinforcement has no significant effect on slope stability when the reinforced soil maintains a high matric suction level. Field instrumentation and numerical analyses have shown that the GBS was effective in minimizing rainwater infiltration into slope during rainfall. Reclaimed asphalt pavement was found to be suitable and sustainable sources to be used as the fine- and coarse-grained materials of GBS.

Uncited reference

Zienkiewicz et al., 2005



(a) Slope with geobags



(b) Slope with GBS

Fig. 12. Slope geometries and boundary conditions used for numerical analyses.

UNCO

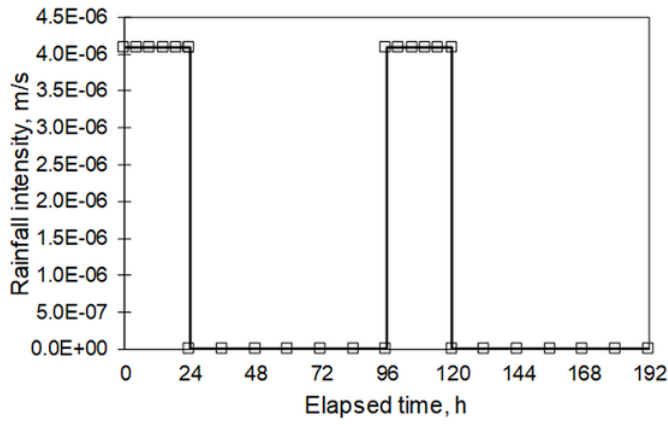


Fig. 13. Rainfall variations applied in numerical analyses.

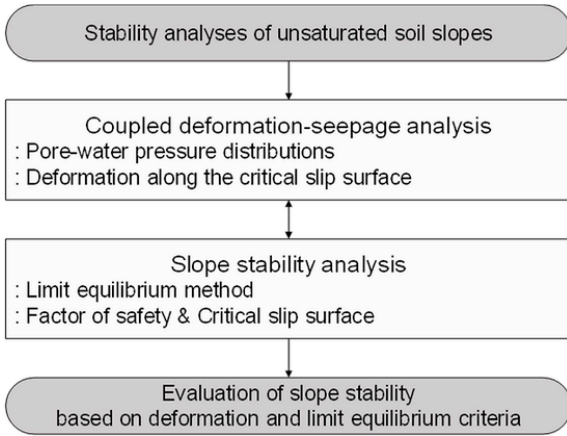


Fig. 14. Numerical analysis procedure for slope stability.

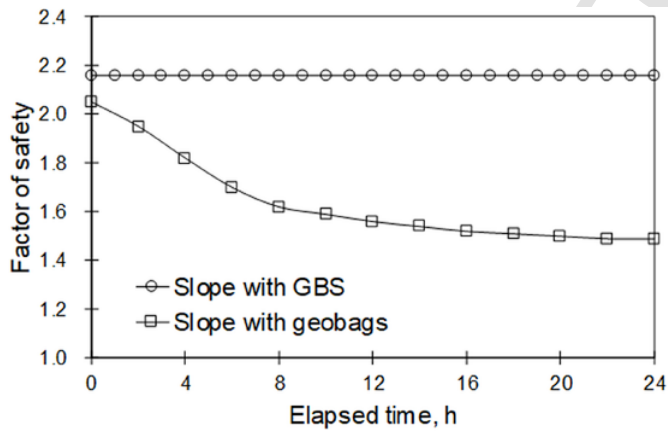


Fig. 15. Variations in factor of safety for the slope covered with GBS and geobags.

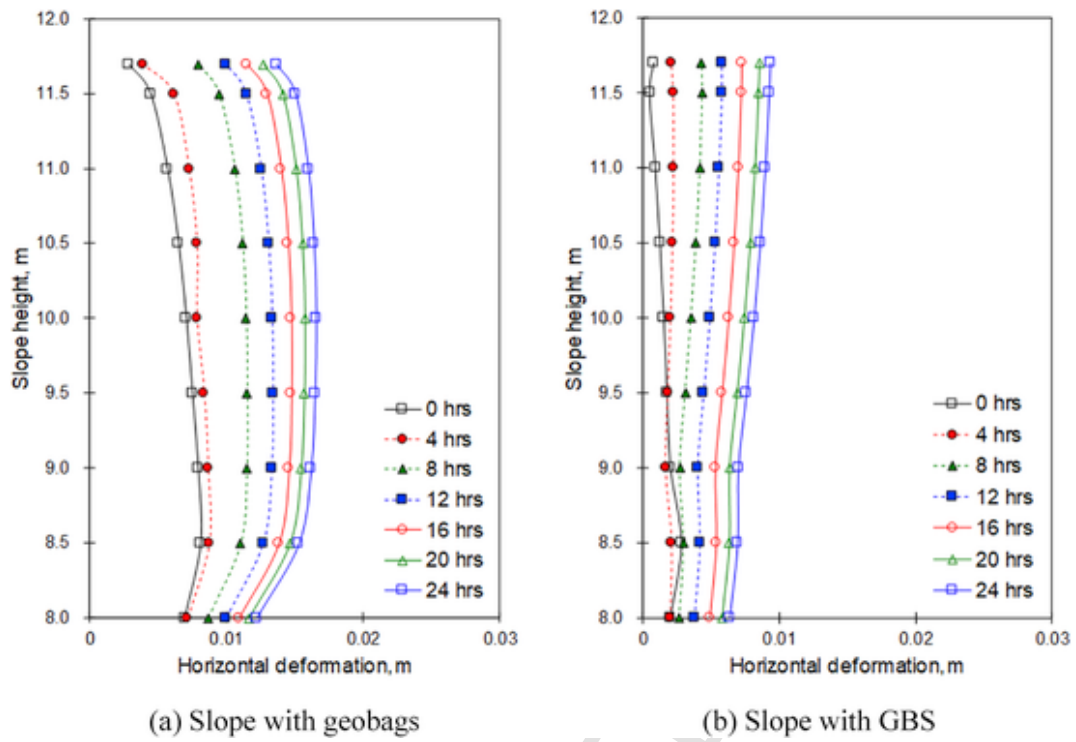
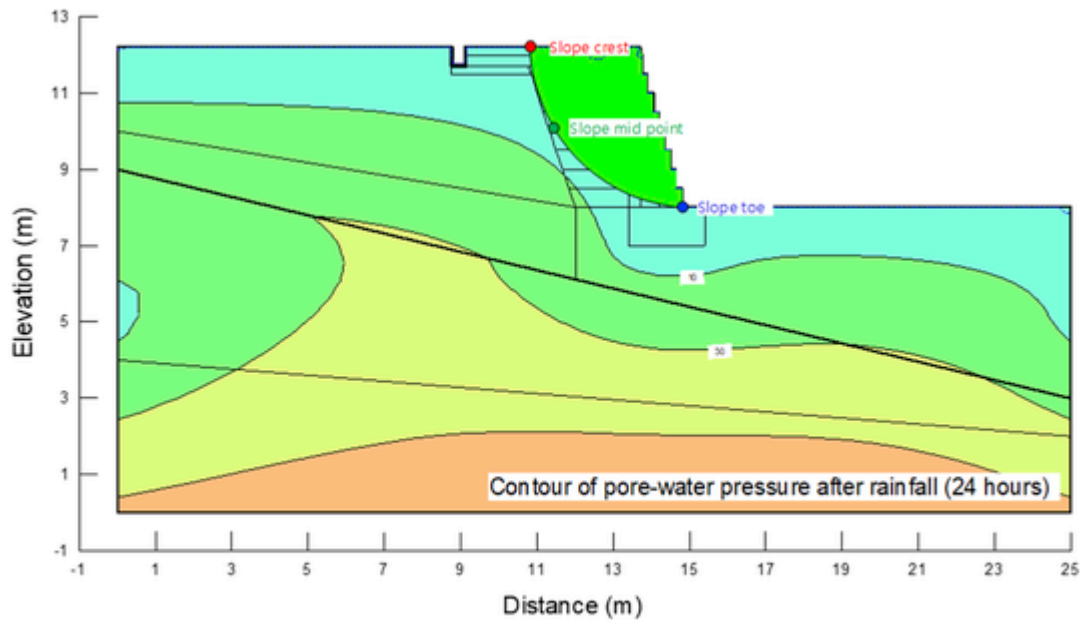
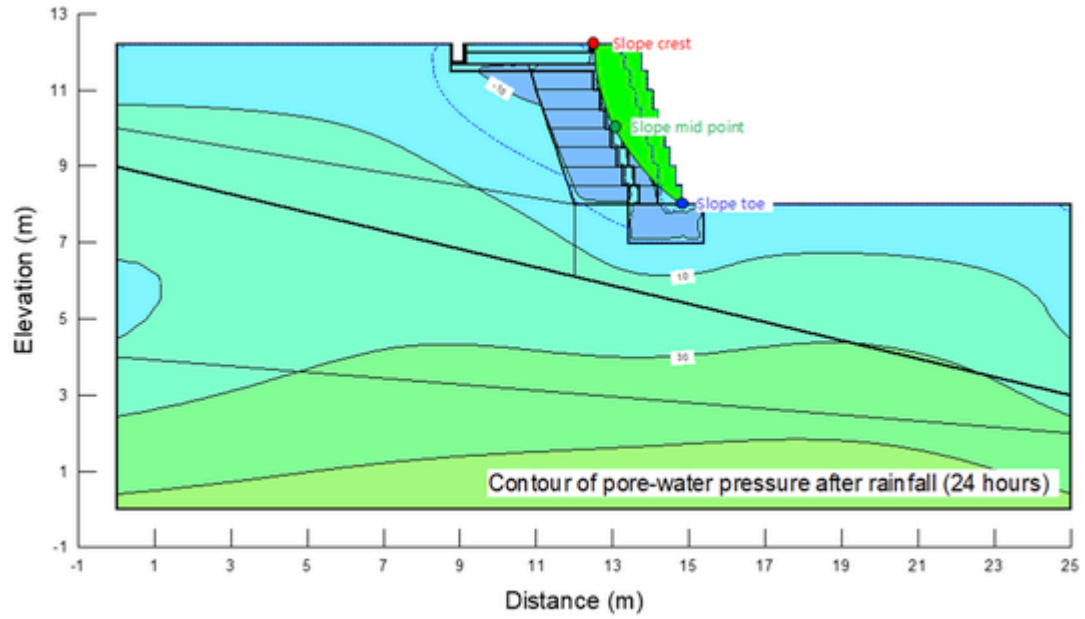


Fig. 16. Horizontal deformation of the slope during rainfall.

UNCORRECTED



(a) Slope with geobags



(b) Slope with GBS

Fig. 17. Distributions of pore-water pressures at the end of rainfall (after 24 h), critical slip surface, and location of the observed deformations on the slope.

UNCG

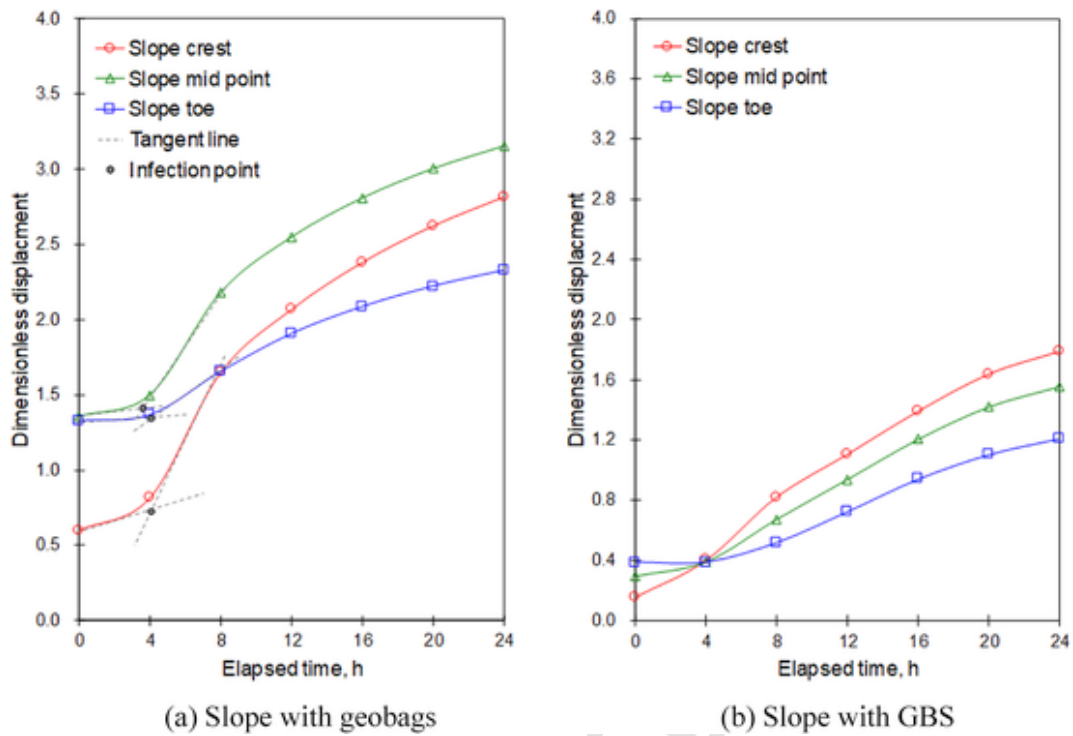


Fig. 18. Dimensionless displacement of the slope during rainfall.

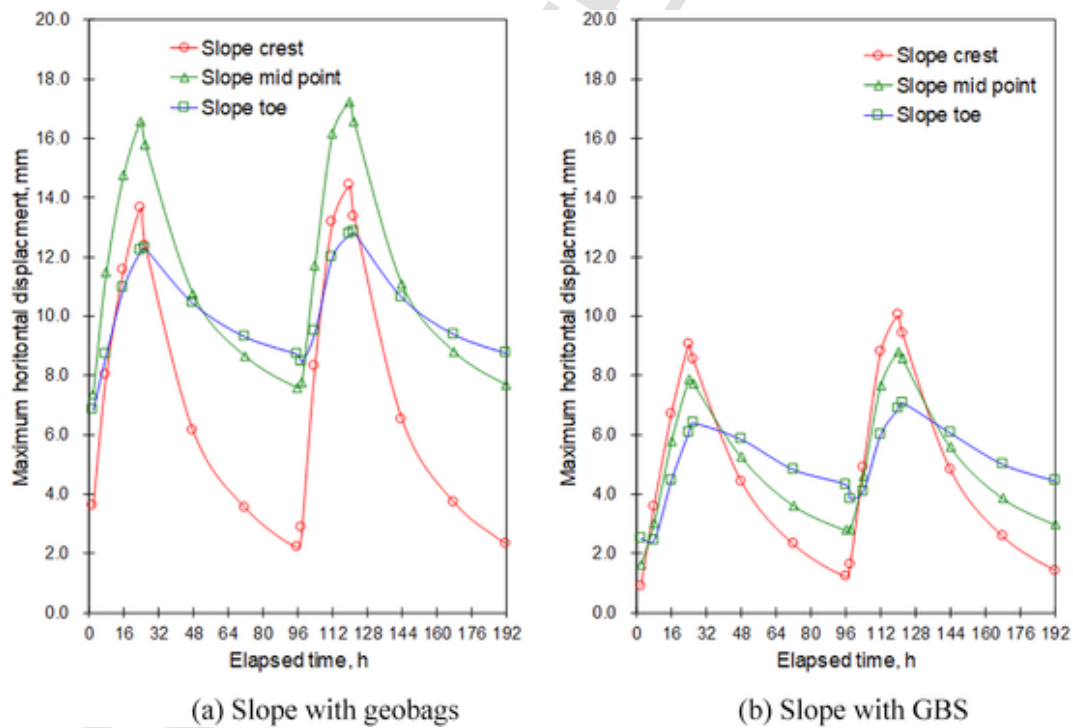


Fig. 19. Maximum horizontal deformation of the slope during the fluctuated rainfall event.

References

AASHTO, 2009. Standard Specifications for Highway Bridges. seventeenth ed.
 Allen, T.M., Bathurst, R.J., 2015. An improved simplified method for prediction of loads in reinforced soil walls. *J. Geotech. Geoenviron.* 141 (11), 04015049.
 Ansari, Y., Merifield, R., Yamamoto, H., Sheng, D., 2011. Numerical analysis of soilbags under compression and cyclic shear. *Comput. Geotech.* 38, 659-688.

ASTM D2487-11, 2011. Standard practice for classification of soils for engineering purposes (unified soil classification system). In: *Annual Book of ASTM Standards*, ASTM International, West Conshohocken, PA.
 ASTM D6838-02, 2008. Standard test methods for the soil-water characteristic curve for desorption using hanging column, pressure extractor, chilled mirror hygrometer, or centrifuge. In: *Annual Book of ASTM Standards*, ASTM International, West Conshohocken, PA.
 Bathurst, R.J., Miyata, Y., Nernheim, A., Allen, A.M., 2008. Refinement of K-stiffness method for geosynthetic-reinforced soil walls. *Geosynth. Int.* 15 (4), 269-295.

- Berg, R.R., Christopher, B.R., Samtani, N.C., 2009. Design and construction of mechanically stabilized earth walls and reinforced soil slopes. In: Federal Highway Administration Report No. FHWA-NHI-10-024FHWA GEC 011.
- Fredlund, D.G., Rahardjo, H., Fredlund, M.D., 2012. Unsaturated Soil Mechanics in Engineering Practice. John Wiley & Sons, Inc.
- Fredlund, D.G., Rahardjo, H., 1993. Soil Mechanics for Unsaturated Soils. John Wiley & Sons, Inc.
- GEOSTUDIO User's Manual, 2012. Geo-Slope International Ltd, Calgary, Alberta, Canada.
- Gofar, N., Hanafiah, H., 2018. Contribution of suction on the stability of reinforced-soil retaining wall. MATEC Web of Conferences, 195, 03004. In: Proceedings of the International Conference on Rehabilitation Method in Civil Engineering (ICRMCE04, 2018) Solo Baru, Indonesia. 11–12 July 2018.
- Khire, M.V., Benson, C.H., Bosscher, P.J., 2000. Capillary barriers: design variables and water balance. *J. Geotech. Geoenviron.* 126 (8), 695–708.
- Kim, Y., Lee, S., Jeong, S., Kim, J., 2013. The effect of pressure-grouted soil nails on the stability of weathered soil slopes. *Comput. Geotech.* 49, 253–263.
- Koerner, R.M., 2005. Designing with Geosynthetics. fifth ed. Prentice Hall.
- Koerner, R.M., Soong, T.Y., 2001. Geosynthetic reinforced segmental retaining walls. *Geotext. Geomembranes* 19 (6), 359–386.
- Lee, K.Z.Z., Chang, N.Y., Ko, H.Y., 2010. Numerical simulation of geosynthetic-reinforced soil walls under seismic shaking. *Geotext. Geomembranes* 28, 317–334.
- Matsuoka, H., Liu, S.H., Yamaguchi, K., 2001. Mechanical properties of soilbags and their application to earth reinforcement. In: Proceedings of the International Symposium on Earth Reinforcement, Fukuoka, Japan. pp. 587–592.
- Matsuoka, H., Liu, S., 2006. A New Earth Reinforcement Method Using Soilbags. Taylor and Francis, London.
- Meteorological Service Singapore, 2015. Annual Climatological Report 2015. Singapore.
- Miyata, Y., Bathurst, R.J., 2007. Development of the K-stiffness method for geosynthetic reinforced soil walls constructed with $c-\phi$ soils. *Can. Geotech. J.* 44 (12), 1391–1416.
- Morgenstern, N.R., Price, V.E., 1965. The analysis of the stability of general slip surfaces. *Geotechnique* 15, 70–93.
- Nicholson, R.V., Gillham, R.W., Cherry, J.A., Reardon, E.J., 1989. Reduction of acid generation in mine tailings through the use of moisture-retaining cover layers as oxygen barriers. *Can. Geotech. J.* 26, 1–8.
- Rahardjo, H., Kim, Y., Gofar, N., Leong, E.C., Wang, C.L., Wong, J.L.H., 2018. Field instrumentations and monitoring of GeoBarrier System for steep slope protection. *Transport. Geotech.* 16, 29–42.
- Rahardjo, H., Santoso, V.A., Leong, E.C., Ng, Y.S., Tam, C.P.H., Satyanaga, A., 2013. Use of recycled crushed concrete and secudrain in capillary barriers for slope stabilization. *Can. Geotech. J.* 50, 1–12.
- Rahardjo, H., Santoso, V.A., Leong, E.C., Ng, Y.S., Tam, C.P.H., Satyanaga, A., 2013. Use of recycled crushed concrete and secudrain in capillary barrier for slope stabilization. *Can. Geotech. J.* 50, 1–12.
- Ren, F., Zhang, F., Wang, G., Zhao, Q., Xu, C., 2018. Dynamic assessment of saturated reinforced-soil retaining wall. *Comput. Geotech.* 95, 211–230.
- Ross, B., 1990. The diversion capacity of capillary barriers. *Water Resour. Res.* 26 (10), 2625–2629.
- Singapore Dept of Statistics, 2015. Statistics Singapore-Latest Data. <http://www.singstat.gov.sg/statistics/latest-data>. (accessed 21 October 2015).
- Stormont, J.C., Anderson, C.E., 1999. Capillary barrier effect from underlying coarse soil layer. *J. Geotech. Geoenviron.* 125 (8), 39–51.
- Tami, D., Rahardjo, H., Leong, E.C., Fredlund, D.G., 2004. A physical model for sloping capillary barriers. *Geotech. Test J.* 27 (2), 173–183.
- Wright, S.G., Duncan, J.M., 1991. Limit equilibrium stability analysis for reinforced slopes. *Transp. Res. Rec.* 1330 (12), 40–46. Transportation Research Board, Washington, D.C.
- Yoo, C., Jung, H.Y., 2006. Case history of geosynthetics reinforced segmental retaining wall failure. *J. Geotechn. Geoenviron.* 132 (12), 1532–1548.
- Yoo, C., 2011. Effect of rainfall on performance of reinforced earth wall. In: Proceedings of Geo-Frontiers 2011: Advances in Geotechnical Engineering, GSP, 211. pp. 1852–1861.
- ~~Zienkiewicz, O.C., Taylor, R.L., Nithiarasu, P., 2005. The Finite Element Method, sixth ed. Butterworth Heinemann.~~
- Zhai, Q., Rahardjo, H., 2012. Determination of soil-water characteristic curve variables. *Comput. Geotech.* 42, 37–43.